AUTOMATED CALCULATION OF CLOUD COVER FROM RGB COMPOSITE OF LANDSAT 8 AND DIWATA-1 SATELLITE IMAGERY

Mc Guillis Kim Ramos[1*], Benjamin Joseph Jiao[2], Romer Kristi Aranas[3], Benjamin Jonah Magallon[4], Jerine Amado[5], Mark Edwin Tupas[6], Ayin Tamondong[7]
[1-7]Department of Geodetic Engineering, University of the Philippines, Diliman, Quezon City, Philippines 1101,
Email: mc_guillis_kim.ramos@upd.edu.ph[1], bdjiao@upd.edu.ph[2], rdaranas@upd.edu.ph[3],
jaamado@upd.edu.ph[4], matupas@upd.edu.ph[5], amtamondong@upd.edu.ph[6]
[4]Department of Cosmosciences, Graduate School of Science, Hokkaido University, 5 Chome Kita 8 Jonishi, Kita Ward, Sapporo, Hokkaido Prefecture 060-0808, Japan
Email: benjamin@ep.sci.hokudai.ac.jp

KEY WORDS: Automated Cloud Cover, Otsu Method, Image Segmentation

ABSTRACT: This paper presents an automated process of determining cloud cover percentage that is sensor independent and works with optical RGB satellite images. The algorithm directly calculates the cloud cover percentage from raw Digital Numbers (DN) of Landsat 8 and Diwata-1 satellite images which results in shorter computation time as it only uses red, green, and blue bands. It defines cloud properties based on how clouds are distinguished by the human eye and uses the Otsu Method as a global thresholding method to separate cloud pixels. The performance of the algorithm is compared to manually generated mask, and the Automatic Cloud Cover Assessment (ACCA) algorithm on Landsat images. The algorithm captured most true cloud pixels as the ACCA without including highly reflective surface features such as the lahar and roads in the classification. However, the algorithm misclassifies thin clouds and sparse clouds. Cloud cover for Landsat image is overestimated since bright features near true cloud pixels are also misclassified as cloud. As for the implementation on the Diwata-1 images, most true cloud pixels are captured by this algorithm. This method however, underestimates cloud cover since cirrocumulus clouds or thin clouds are not identified as clouds. In conclusion, RGB band are sufficient to estimate cloud cover of satellite images with less processing steps and shorter computation time than other methods. This method can be used for fast and automated calculation of cloud cover for quicklook assessment or target capturing.

1. INTRODUCTION

Cloud cover is a basic information stored in metadata and is used as discriminator when downloading satellite and aerial images. Although clouds take an essential role in weather and climate studies, most earth-observation satellites consider them as contaminants and are often masked out when doing surface feature analysis and data product generation. Clouds and cloud shadows not only block view for surface underlying it, but it also affects spectral information which in turn will produce skewed surface information used in atmospheric correction, calculation of Normalized Difference Vegetation Index, land cover, etc (Zhu, Woodcock, 2012). Determination of an accurate cloud cover for satellite images is therefore essential to determine image utility and image quality and evaluation of satellite images that can be salvaged and used for further data analysis.

Cloud mask generation procedures work by using cloud properties which includes having a colder temperature, higher reflectance and higher altitude than other surface features(Gomez-Chova et al, 2007). Several methods are already established producing excellent cloud masks which are done before using images for data product generation. Commercial cloud masks although can be used to various satellites applying the same concept, they are generally formulated to cater specific satellites making use of all possible bands available for accurate determination. MOD35 for example is a cloud mask algorithm formulated for MODIS images which uses 19 channels for its cloud mask. The Automatic Cloud Cover Assessment (ACCA) by Irish et. Al (2006) from the Goddard Space Flight Center of NASA is a method developed for Landsat 7. As Landsat 7's primary goal to archive cloudless Earth images, the cloud cover for each image is evaluated and stored as a metadata used for archiving. The ACCA algorithms follows the general cloud properties which is that clouds appear white, bright, and are colder than land surfaces. The algorithm uses three visible bands, a shortwave infrared band, and thermal infrared band. Zhu, Wang and Woodcock (2015) presented an improvement to the F-mask algorithm of the two later authors (2012) which requires fewer bands and applied to Landsat 4-7 and Sentinel images. They used cirrus band in place of the thermal band where the method detects cloud and cloud shadows from probability mask and scene-based threshold. The resulting cloud masks are more sensitive to thin clouds and cloud shadows. However, as mentioned most of these require specific bands such as infrared and thermal infrared which is essential to discriminate the cold temperature of clouds from cloud surfaces

such as snow. This presents a problem for earth-observation satellite that are confined to the visible and near-infrared domain.

In this paper, an automated method of determining cloud cover percentage using red, green and blue bands is presented and tested on Landsat 8 images and Diwata-1 images. Aside from using only three visible bands, this method requires minimal pre-processing as it uses raw DN values which therefore presents ease in computation ideal for on-board satellite calculations. This method can be applied to other satellite payloads for quicklook generation for assessment, scheduling and target capturing of a particular scene.

2. RELATED LITERATURE

To eliminate the dependency on thermal bands, several algorithms that try to capture clouds with limited bands as possible were reviewed and enhanced by incorporating image enhancement procedures. Braaten et al, (2015) designed a cloud and cloud shadow algorithm for Landsat MSS which has only four bands ranging from 0.5µm to 1.1 µm. It identifies cloud by combining Top of the Atmosphere corrected bands and incorporating Digital elevation model and then applying thresholds for cloud, water and cloud shadow identification. The method showed an accuracy of 84% when compared to the Fmask algorithm. The difference is due to omission of thin clouds and bright shadows. Richter (2008) also presented an improved atmospheric correction for multispectral VNIR satellite images by first identifying cloud over a scene. Although these methods work for cloud determination, they require a detailed analysis of spectral responses of the images. Another simple and effective method of cloud determination is using image segmentation.

Automated feature extraction using thresholding is based on manual differentiation of feature and background where threshold used is visually assessed if it is able to truthfully discriminate preferred feature. Manual processing is time consuming but it produces a more accurate result than most automated methods. The researchers aim to mimic, automate, and apply this manual process to cloud detection as it is an image segmentation procedure. Like any other method, accuracy of the segmentation depends on the band combination that would accentuate clouds and a proper threshold to differentiate clouds from non-clouds. However, when cloud signals are hard to differentiate with other features, image enhancements techniques are usually done. Dev, Lee and Winkler (2016) presented a method of cloud determination using image segmentation from sky/cloud images. They developed a cloud signature for different color models and applied a partial least square regression analysis. Their analysis shows that saturation and blue-to-red ratios are more suitable for cloud segmentation which demonstrate that specific color components works better than others.

Hue-Saturation-Intensity is one of the color models that is suited to describe color for human interpretation (Gonzales, Woods, 2008). Although human eye is perceptive to red, green and blue, they are more used for machine implementations. When describing colors descriptors used are hue (purity of the color), saturation (dilution of color from white light) and intensity. This model makes it suitable for segmentation, fusion, recognition, color enhancement and color-based object detection (Chien, 2011).

Zhang and Xiao (2012) proposed a method using HSI color model to discriminate clouds from aerial photographs. Their method is based on human-perception of clouds where clouds have higher intensity and lower saturation and hue values compared to non-cloud regions. Aside from image enhancement from using HSI model, their method proposed an optimal thresholding method to separate cloud pixels. Zhang and Xiao method was used as the basis of this paper for the automated cloud cover algorithm.

3. METHODS

3.1. Dataset

Level 1 images of the Landsat 8 Operational Land Imager (OLI) was used as dataset where band 4 (0.64-0.67µm), band 3 (0.53-0.59µm) and band 2 (0.45-0.51µm) was used to create RGB composite image. Raw Medium Field Camera (MFC) and High Precision Telescope (HPT) RGB composites was directly used for this cloud cover algorithm with spatial resolution of 185m and 3m, respectively. Locations of satellite images chosen as study areas for both Landsat and Diwata-1 images is shown in Figure 1. Images were also chosen based on the amount of cloud cover where both thin and thick clouds can be evaluated.

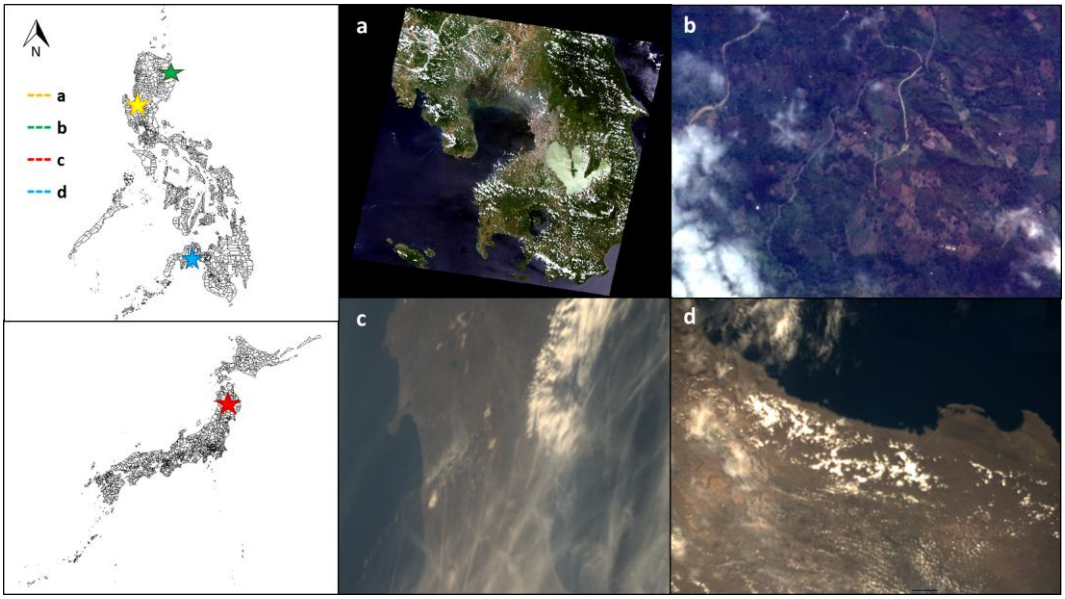

Figure 1. Locations of selected study areas acquired from Landsat (a), Diwata-1 HPT (b) and Diwata-1 MFC (c-d) satellite images.

3.2. Framework for Cloud Cover Percentage determination

The basis of the cloud cover algorithm is adapted on how clouds are manually identified with basis from color, structure and location. The construction of the cloud cover algorithm is based on the following defined cloud properties:

1. Clouds generally appear white which results in higher intensity and lower hues than most surface features.
2. Cloud covered regions appear flat than the surface features.
3. Clouds are clustered and do not come in sparkle cloud pixels.

Based on these assumptions, we enhance the candidate cloud pixels and choose a suited threshold that is scene and image dependent. Figure 2 shows the workflow of the cloud cover algorithm. The algorithm is implemented in Python 2.7 with dependencies on OpenCV, Numpy and GDAL libraries.

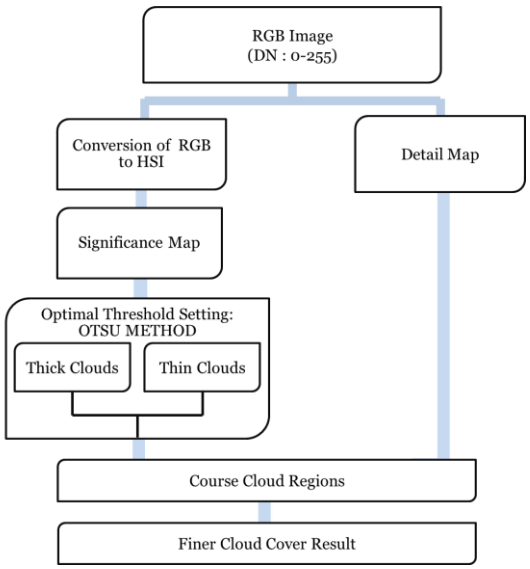

Figure 2. Workflow of the cloud generation procedure using RGB composite images. This framework is adapted from the cloud refinement scheme of Zhang and Xiao (2012)

3.2.1. Conversion to Hue/Saturation/Intensity (HSI)

To better visualize and differentiate clouds, RGB composite is converted to HSI color model given by equations 1 – 4 (Gonzales, 2008) where H, S and I correspond to the Hue, Saturation and Intensity values, respectively. For better visualization H,S and I were normalized to [0,1]. Figure 3 shows the corresponding Intensity and Hue values of Landsat image.

$$\theta = cos^{-1}\left\{\frac{{}^{1}/_{2}[(R-G)+(R-B)]}{[(R-G)^2+(R-B)(G-B)]^{1/2}}\right\} \quad (1)$$

$$H = \begin{cases} \theta & if\ B \geq G \\ 360 - \theta & if\ B > G \end{cases} \quad (2)$$

$$S = 1 - \frac{3}{(R+G+B)}[\min(R,G,B)] \quad (3)$$

$$I = \frac{1}{3}(R+G+B) \quad (4)$$

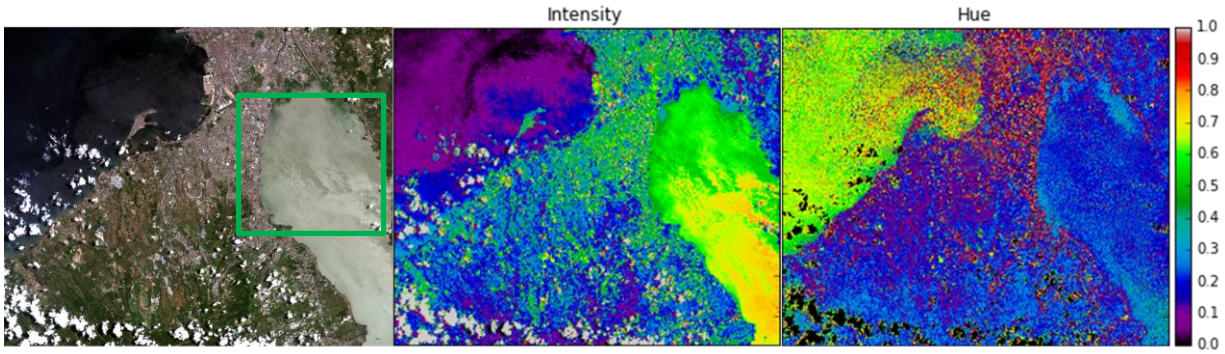

Figure 3. Landsat RGB composite image and corresponding Intensity and Hue from HSI model.

Inspecting the RGB composite, cloud can be distinguished as it appears very white compared to other surface features. However, lahar (highlighted green) although with a reduced scale, also appear white and bright which can be mistaken as cloud in classification. Inspecting the intensity and hue values, distinction of clouds can be easily seen as clouds intensity appear white and bright with intensity of >80% and at the same time, have low hue values (< 10%) that appears black in the image. With this observation, clouds can be enhanced by creating a significance map (W) using equation

$$W = \frac{I+e}{H+e} \quad (5)$$

Where *I*, *H* and *e* are the normalized intensity value, normalized hue value and amplification factor, respectively. The amplification factor for all images are set to 1. Figure 4 shows the produced significance map where the clouds are more distinguishable from the non-cloud pixels. This step is crucial as it influences threshold selection that would accurately identify cloud pixels and as much as possible limit inclusion of non-cloud pixels in the classification. Range of Significance map was set to [0,255].

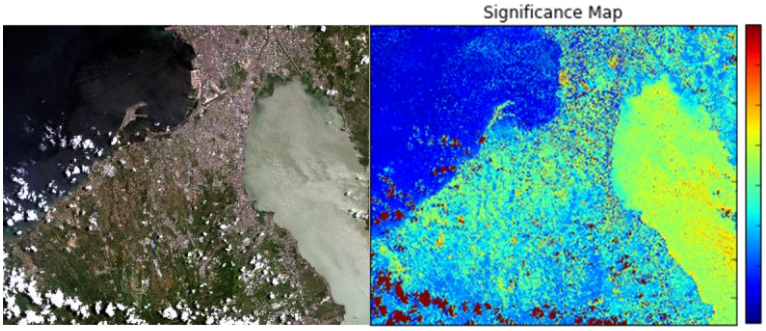

Figure 4. Produced Significance Map accentuating clouds from other surface features (colored red).

3.2.2. Global Thresholding using Otsu Method

After creation of the Significance Map, the cloud mask can be created by choosing a threshold that would accurately identify true cloud pixels. One automated process of choosing threshold is the Otsu method which is a global thresholding method that looks on the histogram of an image. The Otsu Method assumes that the image has bi-modal histogram which corresponds to the foreground (clouds) and background (non-clouds). Instead of minimizing the variance between classes, the Otsu methods maximizes the variance between-classes such that threshold *k* is the value that best separates the two classes given in equation 6. Complete derivation of the Otsu method is in (Otsu, 1979).

$$\sigma_B^2(k^*) = max_{0<k<L-1}\, \sigma_B^2(k) \tag{6}$$

It is observed that the Otsu Method fails when the image has a unimodal histogram. To capture all cloud pixels and minimize inclusion of non-cloud pixels, an observed minimum value for threshold is set to 130. A coarse cloud mask is then created by taking pixels greater than the set optimal threshold (equation 8).

$$T^{Optimal} = \begin{cases} 130, & k < 130 \\ k, & k > 130 \end{cases} \tag{7}$$

$$Cloud^{Coarse} = \begin{cases} 0, & W < T^{Optimal}\ (non-cloud) \\ 1, & W \geq T\ (cloud) \end{cases} \tag{8}$$

This coarse cloud condition works well to capture thick clouds for both Landsat and Diwata-1. However, thin clouds are excluded in the classification. Hence another filter is added by looking at the Intensity and Hue values (equation 9).

$$Cloud_{thin} = \begin{cases} 1, & I_{thin} \geq 130 \ \cap \ H_{thin} \leq 170 \\ 0, & otherwise \end{cases} \tag{9}$$

3.2.3. Detail Map Generation

Although thresholds are set to capture all clouds in the scene, bright features are still included in the classification. Using the third cloud property, misclassified pixels due to surface features such as building and roads can be separated by determining their locations from a detail map. A detail layer D is constructed by subtracting image I from the bilateral-filtered image I`. Multilayer Detail map $\{D_j\}_{j=1}^{M}$ is then constructed following equation 10

$$D_j = I'_j - I'_{j-1} \tag{10}$$

where I'_0 is the original image. For this paper, M is set to 4 layers. Finally, a weighted sum of the M details layers $\{D_j\}_{j=1}^{M}$ is computed creating detail map I^{Detail}. Otsu threshold T^{Detail} was used to separate pixels with strong edges and background. From these we construct $Cloud^{detail}$ using equation 11.

$$Cloud^{detail} = \begin{cases} 1, & < T^{Detail}\ (cloud) \\ 0, & otherwise\ (non-cloud) \end{cases} \tag{11}$$

3.2.4. Cloud Mask Generation

Candidate cloud pixels identified from the global thresholding are then intersected with the mask created from the detail map. From this mask, the cloud cover percentage of the image is calculated using the equation

$$\%\ cloud\ cover\ = \frac{number\ of\ cloud\ pixels}{total\ number\ of\ pixels}\ X\ 100\% \qquad (5)$$

3.3. Validation

2.3.1. Manual Cloud Mask Generation

The manual mask generation was implemented in ENVI 5.1. First, classes were produced using the K-means unsupervised classification of ENVI. The number of classes was set to 20 or higher depending on the image in order to create a fine classification. Then, cloud mask was created by manually selecting potential cloud classes. The cloud mask was further refined by manually removing falsely classified cloud.

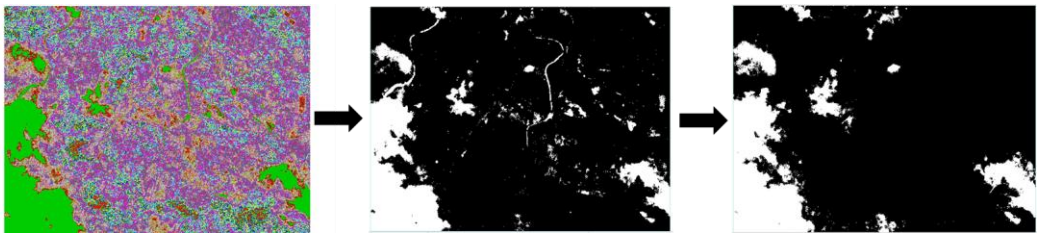

Figure 5. Manual Mask Generation. (A) shows the classes produced from K-means classification. (B) is the mask produced from selected cloud classes and final cloud mask (C) from manual filtering misclassified pixels.

3.3.2 Automatic Cloud Cover Assessment

ACCA algorithm was used to validate the cloud mask produced from Landsat images. It works by examining the data 2 times: pass-one comprising of 8 filters where true cloud pixels are identified, and the second pass where missed cloud pixels are identified from statistical information from pass-1. The step-by-step method of Irish et. Al was followed and encoded in Python 2.7 where produced cloud mask was compared with the cloud mask produced from RGB Landsat image.

3.3.3. Performance Evaluation

Cloud mask produced from this method is compared side by side with the manually generated mask by identifying correctly classified pixels (True Cloud and True Non-cloud) and misclassified pixels (False Cloud and False Non-cloud).

4. RESULTS

4.1. Algorithm Assessment

Figure 6 shows the cloud mask created for Landsat images. Comparing with the RGB images, cloud mask generated captured most cloud pixels. Figure 6a shows the performance of cloud mask over land and water where only true clouds are included in the classification. The same performance is seen for clouds with highly reflective surface (figure 6b) where algorithm was also able to capture sparse clouds. On figure 6c, true cloud pixels are still captured without including highly reflective urban area (highlighted yellow). However, evident misclassification of lahar can be observed. This is due to the added condition to capture thin clouds. Since conditions are based on looking at intensity and hue values, some highly reflective features can exhibit the same values as thin clouds which will be included in the classification. Comparing with the ACCA algorithm, the cloud mask produced from this method

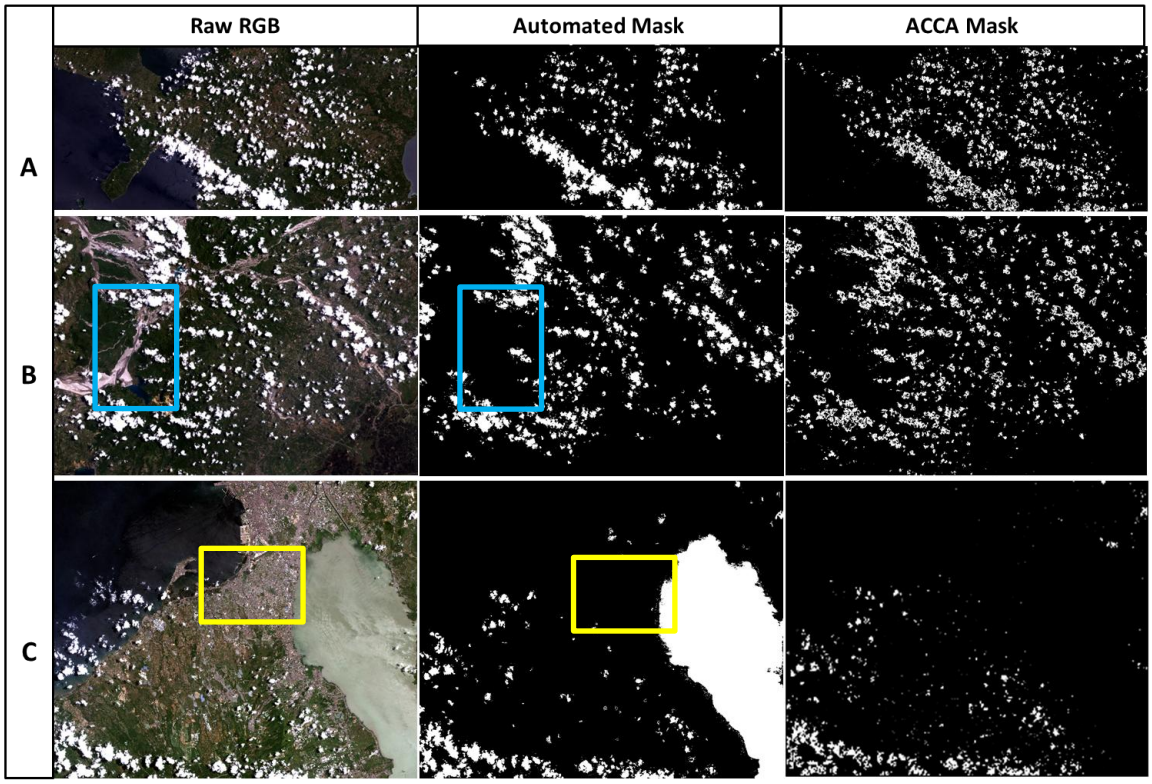

Figure 6. Comparison of Cloud mask generated from this method and ACCA algorithm for various scenes of Landsat images.

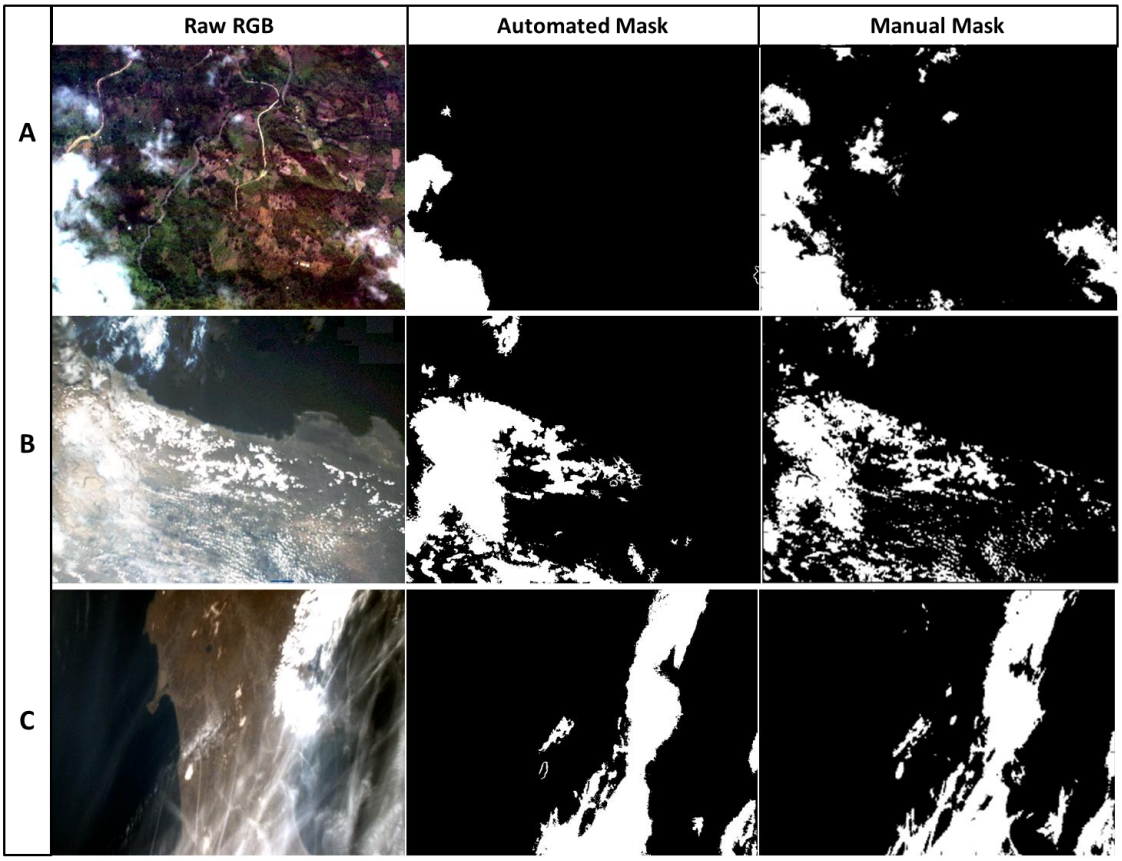

Figure 7. Comparison of Cloud mask generated from this method and manual mask for (a) High Precision Telescope image and (b-c) Medium Field Camera images of Diwata-1.

gave comparable results capturing true cloud pixels with a lesser computing time. The advantage of this technique is that it does not suffer from omission errors which is present to the cloud mask of ACCA even when evaluating relatively think and opaque clouds. The straight-forward procedure of pixel-by-pixel evaluation of this method can easily classify clouds unlike the scene averaging method ACCA which led to holes within its cloud mask.

Cloud mask algorithm applied on Diwata-1 images is seen in figure 7. Compared to the Landsat images, Diwata-1 suffers from image contrast which directly affects the selection of threshold for cloud identification. However, for both HPT image (figure 7a) and MFC image (figure 7b and 7c) with different spectral and spatial resolution, most thick clouds are still correctly included in the cloud mask. Performance of cloud evaluation gives the same observation with the Landsat where it does not classify land and water to the cloud mask. Although for the three images presented, they all suffer from exclusion of most cirrus or thin clouds. Although additional condition was added to capture thin clouds, thresholds set are still insufficient to capture all thin clouds without bringing in too much false cloud pixels from other bright features of the image. Manual cloud mask generated for Diwata-1 images are based from the images with enhanced contrast.

4.2 Validation

A confusion matrix for all images was created (Table 1) to quantify the performance of the algorithm. The accuracy of the algorithm ranges around 90% for both Landsat and Diwata-1 which indicates overall capability in identifying true cloud pixels and true non-cloud pixels. The algorithm works well in identifying non-cloud pixels with almost 100% specificity and high negative predicted value. Sensitivity computed for Landsat appears to be average however, it is established from the discussion that this is due to the disadvantage of ACCA for pixel evaluation. The varying sensitivity values for Diwata-1 is due to the amount of thin clouds of the images which the algorithm fails to capture. Apart from that, the algorithm is able to give reliable results which is indicated by the low false discovery rate, false omission rate and, fall-out.

Table 1. Summary of performance evaluation of Automated Cloudmask from ACCA and Manual Mask.

		Accuracy	*Precision*	*Negative Predicted Value*	*Sensitivity*	*Specificity*	*False Discovery Rate*	*False Omission Rate*	*Fall-Out*	*Miss Rate*
Landsat	***A***	0.94	0.75	0.95	0.44	0.99	0.25	0.05	0.01	0.56
	B	0.93	0.76	0.94	0.42	0.99	0.24	0.06	0.01	0.58
	C	0.82	0.09	0.98	0.55	0.83	0.91	0.02	0.17	0.45
Diwata-1	***A***	0.91	1.00	0.90	0.43	1.00	0.00	0.10	0.00	0.57
	B	0.93	0.77	0.97	0.86	0.94	0.23	0.03	0.06	0.14
	C	0.97	0.95	0.97	0.87	0.99	0.05	0.03	0.01	0.13

5. CONCLUSION

Although various methods are available for cloud cover assessment, this method demonstrates the comparable performance of using image segmentation of clouds from the basic RGB composite. This presents an automated process of cloud determination that can be used for any satellite image with varying spatial and spectral resolution. From the evaluation of the produced mask, the method is able to perform well with identifying cloud pixels and non-cloud pixels and giving a fair estimate of cloud cover over a scene. It also exhibited comparable results with established cloud cover method such as the ACCA. However, unlike analytic methods of cloud determination, this sometimes fails to accurately distinguish clouds with comparably bright surface features and identification of thin clouds. Although algorithm works well with any satellite image, performance can be enhanced if thresholds are optimized based on the images produced by a specific payload of satellite to create a more exact estimate of cloud cover for image processing and product generation.

6. ACKNOWLEDGMENT

This work is supported by the Department of Science and Technology - Philippine Council of Industry, Energy, and Emerging Technology Research and Development (DOST-PCIEERD) under the Development of the Philippine Scientific Earth Observation Microsatellite (PHL-MICROSAT – Project 3) Program.

7. REFERENCES

References from Journals:

Zhu, Z, Woodcock,C. E., 2012, Object Based Cloud and Cloud Shadow Detection in Landsat Imagery, *Remote Sensing of Environment*, 118, pp. 83-94.

Gomez-Chova, et. Al., 2007. Cloud Screening Algorithm for ENVISAT/MERIS Multispectral Image. IEEE Transactions of Geoscience and Remote Sensing, Vol. 45 No. 12, pp. 4105 – 4118.

Irish, R.R., Barker, J. L., Goward, S. N., Arvidson, T., 2006, Characterization of the Landsat-7 ETM+ Automated Cloud Cover Assessment Algorithm, *Photogrammetric Engineering anf Remote Sensing, pp.* 1179-1188

Zhu, Z., Wang, S., Woodcock, C., 2015. Improvement and Expansion of the F-mask Algorithm: cloud, cloud shadow and snow detection for Landsat 4-7 and Sentinel 2 images. Remote Sensing of Environment 159, pp. 269 – 277.

Braaten, J. D., Cohen, W.B., Yang, Z. , Automated Cloud and Cloud Shadow Identification for Landsat MSS Imagery for Temperate Ecosystems. Remote Sensing of Environment 169, pp. 128-138.

Richter, R., 2008. Classification Metrics for Improved Atmospheric Correction of VNIR Imagery. Sensors, 8, pp. 6999-7011.

Dev, S., Lee, Y. H., Winkler, S., 2016. Color-Based Segmentation of Sky/Cloud Images from Ground-based Cameras. IEEE Journal of Selected topics in Applied Earth Observations and Remote Sensing.

Gonzales, R. C., Woods, R. E., Digital Image Processing, 3rd Edition, Prentice Hall, Upper Saddle River, NJ 07458.

Chien, C.L., Tseng, D. C., 2011. Color Image Enhancement with Exact HSI Color Model. ICIC International ISSN 1349 – 4198, pp 6699-6710.

Zhang, Q., Xiao, C., 2014. Cloud Detection of RGB Color Aerial Photographs by Progressive Refinement Scheme. IEEE Transactions on Geoscience and Remote Sensing, Vol. 25, 7264 – 7275.

Otsu, N., (1979). A Threshold Seleting Method from Gray-level Histograms. IEEE Transactions on Systems, Man and Cybernetics, Vol. SMC-9, pp. 62 – 66.